Scalar quark searches in e^+e^- collisions at $\sqrt{s} = 181 - 184$ GeV

The ALEPH Collaboration

Abstract

Searches for scalar top, scalar bottom and degenerate scalar quarks have been performed with data collected with the ALEPH detector at LEP. The data sample consists of 57 pb^{-1} taken at $\sqrt{s}$ = 181–184 GeV. No evidence for scalar top, scalar bottom or degenerate scalar quarks was found in the channels $\tilde{t} \to c\chi$, $\tilde{t} \to b\ell\tilde{\nu}$, $\tilde{b} \to b\chi$, and $\tilde{q} \to q\chi$. From the channel $\tilde{t} \to c\chi$ a limit of 74 GeV/c^2 has been set on the scalar top quark mass, independent of the mixing angle. This limit assumes a mass difference between the $\tilde{t}$ and the χ in the range 10–40 GeV/c^2. From the channel $\tilde{t} \to b\ell\tilde{\nu}$ the mixing-angle-independent scalar top limit is 82 GeV/c^2, assuming $m_{\tilde{t}} - m_{\tilde{\nu}} > 10$ GeV/c^2. From the channel $\tilde{b} \to b\chi$, a limit of 79 GeV/c^2 has been set on the mass of the supersymmetric partner of the left-handed state of the bottom quark. This limit is valid for $m_{\tilde{b}} - m_{\chi} > 10$ GeV/c^2. From the channel $\tilde{q} \to q\chi$, a limit of 87 GeV/c^2 has been set on the mass of supersymmetric partners of light quarks assuming five degenerate flavours and the production of both "left-handed" and "right-handed" squarks. This limit is valid for $m_{\tilde{q}} - m_{\chi} > 5$ GeV/c^2.

The ALEPH Collaboration

R. Barate, D. Buskulic, D. Decamp, P. Ghez, C. Goy, S. Jezequel, J.-P. Lees, A. Lucotte, F. Martin, E. Merle, M.-N. Minard, J.-Y. Nief, B. Pietrzyk

Laboratoire de Physique des Particules (LAPP), IN^{2}P^3-CNRS, F-74019 Annecy-le-Vieux Cedex, France

R. Alemany, G. Boix, M.P. Casado, M. Chmeissani, J.M. Crespo, M. Delfino, E. Fernandez, M. Fernandez-Bosman, Ll. Garrido,[15] E. Graugès, A. Juste, M. Martinez, G. Merino, R. Miquel, Ll.M. Mir, P. Morawitz, I.C. Park, A. Pascual, I. Riu, F. Sanchez

Institut de Física d'Altes Energies, Universitat Autònoma de Barcelona, 08193 Bellaterra (Barcelona), E-Spain[7]

A. Colaleo, D. Creanza, M. de Palma, G. Gelao, G. Iaselli, G. Maggi, M. Maggi, S. Nuzzo, A. Ranieri, G. Raso, F. Ruggieri, G. Selvaggi, L. Silvestris, P. Tempesta, A. Tricomi,[3] G. Zito

Dipartimento di Fisica, INFN Sezione di Bari, I-70126 Bari, Italy

X. Huang, J. Lin, Q. Ouyang, T. Wang, Y. Xie, R. Xu, S. Xue, J. Zhang, L. Zhang, W. Zhao

Institute of High-Energy Physics, Academia Sinica, Beijing, The People's Republic of China[8]

D. Abbaneo, U. Becker, P. Bright-Thomas, D. Casper, M. Cattaneo, V. Ciulli, G. Dissertori, H. Drevermann, R.W. Forty, M. Frank, F. Gianotti, R. Hagelberg, J.B. Hansen, J. Harvey, P. Janot, B. Jost, I. Lehraus, P. Maley, P. Mato, A. Minten, L. Moneta,[20] N. Qi, A. Pacheco, F. Ranjard, L. Rolandi, D. Rousseau, D. Schlatter, M. Schmitt,[1] O. Schneider, W. Tejessy, F. Teubert, I.R. Tomalin, M. Vreeswijk, H. Wachsmuth

European Laboratory for Particle Physics (CERN), CH-1211 Geneva 23, Switzerland

Z. Ajaltouni, F. Badaud G. Chazelle, O. Deschamps, A. Falvard, C. Ferdi, P. Gay, C. Guicheney, P. Henrard, J. Jousset, B. Michel, S. Monteil, J-C. Montret, D. Pallin, P. Perret, F. Podlyski, J. Proriol, P. Rosnet

Laboratoire de Physique Corpusculaire, Université Blaise Pascal, IN^{2}P^3-CNRS, Clermont-Ferrand, F-63177 Aubière, France

J.D. Hansen, J.R. Hansen, P.H. Hansen, B.S. Nilsson, B. Rensch, A. Wäänänen

Niels Bohr Institute, 2100 Copenhagen, DK-Denmark[9]

G. Daskalakis, A. Kyriakis, C. Markou, E. Simopoulou, A. Vayaki

Nuclear Research Center Demokritos (NRCD), GR-15310 Attiki, Greece

A. Blondel, J.-C. Brient, F. Machefert, A. Rougé, M. Rumpf, R. Tanaka, A. Valassi,[6] H. Videau

Laboratoire de Physique Nucléaire et des Hautes Energies, Ecole Polytechnique, IN^{2}P^3-CNRS, F-91128 Palaiseau Cedex, France

E. Focardi, G. Parrini, K. Zachariadou

Dipartimento di Fisica, Università di Firenze, INFN Sezione di Firenze, I-50125 Firenze, Italy

R. Cavanaugh, M. Corden, C. Georgiopoulos, T. Huehn, D.E. Jaffe

Supercomputer Computations Research Institute, Florida State University, Tallahassee, FL 32306-4052, USA [13,14]

A. Antonelli, G. Bencivenni, G. Bologna,[4] F. Bossi, P. Campana, G. Capon, F. Cerutti, V. Chiarella, G. Felici, P. Laurelli, G. Mannocchi,[5] F. Murtas, G.P. Murtas, L. Passalacqua, M. Pepe-Altarelli

Laboratori Nazionali dell'INFN (LNF-INFN), I-00044 Frascati, Italy

M. Chalmers, L. Curtis, A.W. Halley, J.G. Lynch, P. Negus, V. O'Shea, C. Raine, J.M. Scarr, K. Smith, P. Teixeira-Dias, A.S. Thompson, E. Thomson, J.J. Ward

Department of Physics and Astronomy, University of Glasgow, Glasgow G12 8QQ,United Kingdom[10]

O. Buchmüller, S. Dhamotharan, C. Geweniger, G. Graefe, P. Hanke, G. Hansper, V. Hepp, E.E. Kluge, A. Putzer, J. Sommer, K. Tittel, S. Werner, M. Wunsch

Institut für Hochenergiephysik, Universität Heidelberg, D-69120 Heidelberg, Germany[16]

R. Beuselinck, D.M. Binnie, W. Cameron, P.J. Dornan,[12] M. Girone, S. Goodsir, E.B. Martin, N. Marinelli, A. Moutoussi, J. Nash, J.K. Sedgbeer, P. Spagnolo, M.D. Williams

Department of Physics, Imperial College, London SW7 2BZ, United Kingdom[10]

V.M. Ghete, P. Girtler, E. Kneringer, D. Kuhn, G. Rudolph

Institut für Experimentalphysik, Universität Innsbruck, A-6020 Innsbruck, Austria[18]

C.K. Bowdery, P.G. Buck, P. Colrain, G. Crawford, A.J. Finch, F. Foster, G. Hughes, R.W.L. Jones, A.N. Robertson, M.I. Williams

Department of Physics, University of Lancaster, Lancaster LA1 4YB, United Kingdom[10]

I. Giehl, C. Hoffmann, K. Jakobs, K. Kleinknecht, M. Kröcker, H.-A. Nürnberger, G. Quast, B. Renk, E. Rohne, H.-G. Sander, P. van Gemmeren, C. Zeitnitz, T. Ziegler

Institut für Physik, Universität Mainz, D-55099 Mainz, Germany[16]

J.J. Aubert, C. Benchouk, A. Bonissent, G. Bujosa, J. Carr,[12] P. Coyle, A. Ealet, D. Fouchez, O. Leroy, F. Motsch, P. Payre, M. Talby, A. Sadouki, M. Thulasidas, A. Tilquin, K. Trabelsi

Centre de Physique des Particules, Faculté des Sciences de Luminy, IN^{2}P^3-CNRS, F-13288 Marseille, France

M. Aleppo, M. Antonelli, F. Ragusa

Dipartimento di Fisica, Università di Milano e INFN Sezione di Milano, I-20133 Milano, Italy.

R. Berlich, V. Büscher, G. Cowan, H. Dietl, G. Ganis, G. Lütjens, C. Mannert, W. Männer, H.-G. Moser, S. Schael, R. Settles, H. Seywerd, H. Stenzel, W. Wiedenmann, G. Wolf

Max-Planck-Institut für Physik, Werner-Heisenberg-Institut, D-80805 München, Germany[16]

J. Boucrot, O. Callot, S. Chen, M. Davier, L. Duflot, J.-F. Grivaz, Ph. Heusse, A. Höcker, A. Jacholkowska, M. Kado, D.W. Kim,[2] F. Le Diberder, J. Lefrançois, L. Serin, E. Tournefier, J.-J. Veillet, I. Videau, D. Zerwas

Laboratoire de l'Accélérateur Linéaire, Université de Paris-Sud, IN^{2}P^3-CNRS, F-91898 Orsay Cedex, France

P. Azzurri, G. Bagliesi,[12] S. Bettarini, T. Boccali, C. Bozzi, G. Calderini, R. Dell'Orso, R. Fantechi, I. Ferrante, A. Giassi, A. Gregorio, F. Ligabue, A. Lusiani, P.S. Marrocchesi, A. Messineo, F. Palla, G. Rizzo, G. Sanguinetti, A. Sciabà, G. Sguazzoni, R. Tenchini, C. Vannini, A. Venturi, P.G. Verdini

Dipartimento di Fisica dell'Università, INFN Sezione di Pisa, e Scuola Normale Superiore, I-56010 Pisa, Italy

G.A. Blair, L.M. Bryant, J.T. Chambers, J. Coles, M.G. Green, T. Medcalf, P. Perrodo, J.A. Strong, J.H. von Wimmersperg-Toeller

Department of Physics, Royal Holloway & Bedford New College, University of London, Surrey TW20 OEX, United Kingdom[10]

D.R. Botterill, R.W. Clifft, T.R. Edgecock, S. Haywood, P.R. Norton, J.C. Thompson, A.E. Wright

Particle Physics Dept., Rutherford Appleton Laboratory, Chilton, Didcot, Oxon OX11 OQX, United Kingdom[10]

B. Bloch-Devaux, P. Colas, B. Fabbro, G. Faïf, E. Lançon,[12] M.-C. Lemaire, E. Locci, P. Perez, H. Przysiezniak, J. Rander, J.-F. Renardy, A. Rosowsky, A. Roussarie, A. Trabelsi, B. Vallage

CEA, DAPNIA/Service de Physique des Particules, CE-Saclay, F-91191 Gif-sur-Yvette Cedex, France[17]

S.N. Black, J.H. Dann, H.Y. Kim, N. Konstantinidis, A.M. Litke, M.A. McNeil, G. Taylor

Institute for Particle Physics, University of California at Santa Cruz, Santa Cruz, CA 95064, USA[19]

C.N. Booth, S. Cartwright, F. Combley, M.S. Kelly, M. Lehto, L.F. Thompson

Department of Physics, University of Sheffield, Sheffield S3 7RH, United Kingdom[10]

K. Affholderbach, A. Böhrer, S. Brandt, J. Foss, C. Grupen, L. Smolik, F. Stephan

Fachbereich Physik, Universität Siegen, D-57068 Siegen, Germany[16]

G. Giannini, B. Gobbo, G. Musolino

Dipartimento di Fisica, Università di Trieste e INFN Sezione di Trieste, I-34127 Trieste, Italy

J. Putz, J. Rothberg, S. Wasserbaech, R.W. Williams

Experimental Elementary Particle Physics, University of Washington, WA 98195 Seattle, U.S.A.

S.R. Armstrong, A.P. Betteridge, E. Charles, P. Elmer, D.P.S. Ferguson, Y. Gao, S. González, T.C. Greening, O.J. Hayes, H. Hu, S. Jin, P.A. McNamara III, J.M. Nachtman,[21] J. Nielsen, W. Orejudos, Y.B. Pan, Y. Saadi, I.J. Scott, J. Walsh, Sau Lan Wu, X. Wu, G. Zobernig

Department of Physics, University of Wisconsin, Madison, WI 53706, USA[11]

[1]Now at Harvard University, Cambridge, MA 02138, U.S.A.
[2]Permanent address: Kangnung National University, Kangnung, Korea.
[3]Also at Dipartimento di Fisica, INFN Sezione di Catania, Catania, Italy.
[4]Also Istituto di Fisica Generale, Università di Torino, Torino, Italy.
[5]Also Istituto di Cosmo-Geofisica del C.N.R., Torino, Italy.
[6]Supported by the Commission of the European Communities, contract ERBCHBICT941234.
[7]Supported by CICYT, Spain.
[8]Supported by the National Science Foundation of China.
[9]Supported by the Danish Natural Science Research Council.
[10]Supported by the UK Particle Physics and Astronomy Research Council.
[11]Supported by the US Department of Energy, grant DE-FG0295-ER40896.
[12]Also at CERN, 1211 Geneva 23,Switzerland.
[13]Supported by the US Department of Energy, contract DE-FG05-92ER40742.
[14]Supported by the US Department of Energy, contract DE-FC05-85ER250000.
[15]Permanent address: Universitat de Barcelona, 08208 Barcelona, Spain.
[16]Supported by the Bundesministerium für Bildung, Wissenschaft, Forschung und Technologie, Germany.
[17]Supported by the Direction des Sciences de la Matière, C.E.A.
[18]Supported by Fonds zur Förderung der wissenschaftlichen Forschung, Austria.
[19]Supported by the US Department of Energy, grant DE-FG03-92ER40689.
[20]Now at University of Geneva, 1211 Geneva 4, Switzerland.
[21]Now at University of California at Los Angeles (UCLA), Los Angeles, CA 90024, U.S.A.

1 Introduction

In the Minimal Supersymmetric extension of the Standard Model (MSSM) [1], each chirality state of the Standard Model fermions has a scalar supersymmetric partner. The scalar quarks (squarks) $\tilde{\mathrm{q}}_{\mathrm{R}}$ and $\tilde{\mathrm{q}}_{\mathrm{L}}$ are the supersymmetric partners of the left-handed and right-handed quarks, respectively. They are weak interaction eigenstates which can mix to form the mass eigenstates. Since the size of the mixing is proportional to the mass of the Standard Model partner, the lighter scalar top (stop) could be the lightest supersymmetric charged particle. The stop mass eigenstates are obtained by a unitary transformation of the $\tilde{\mathrm{t}}_{\mathrm{R}}$ and $\tilde{\mathrm{t}}_{\mathrm{L}}$ fields, parametrised by the mixing angle $\theta_{\tilde{\mathrm{t}}}$. The lighter stop is given by $\tilde{\mathrm{t}} = \tilde{\mathrm{t}}_{\mathrm{L}} \cos\theta_{\tilde{\mathrm{t}}} + \tilde{\mathrm{t}}_{\mathrm{R}} \sin\theta_{\tilde{\mathrm{t}}}$, while the heavier stop is the orthogonal combination. The stop could be produced at LEP in pairs, $\mathrm{e^+e^-} \to \tilde{\mathrm{t}}\tilde{\mathrm{t}}$, via s-channel exchange of a virtual photon or a Z.

The searches for stops described here assume that all supersymmetric particles except the lightest neutralino χ and possibly the sneutrino $\tilde{\nu}$ are heavier than the stop. The conservation of R-parity is also assumed; this implies that the lightest supersymmetric particle (LSP) is stable. Under these assumptions, the two dominant decay channels are $\tilde{\mathrm{t}} \to \mathrm{c}\chi$ and $\tilde{\mathrm{t}} \to \mathrm{b}\ell\tilde{\nu}$ [2]. The first decay can only proceed via loops and thus has a very small width, of the order of 0.01–1 eV [2]. The $\tilde{\mathrm{t}} \to \mathrm{b}\ell\tilde{\nu}$ channel proceeds via a virtual chargino exchange and has a width of the order of 0.1–10 keV [2]. The latter decay dominates when it is kinematically allowed. The phenomenology of the scalar bottom (sbottom), the supersymmetric partner of the bottom quark, is similar to the phenomenology of the stop. Assuming that the $\tilde{\mathrm{b}}$ is lighter than all supersymmetric particles except the χ, the $\tilde{\mathrm{b}}$ will decay as $\tilde{\mathrm{b}} \to \mathrm{b}\chi$. Compared to the $\tilde{\mathrm{t}}$ decays, the $\tilde{\mathrm{b}}$ decay has a large width of the order of 10–100 MeV. Direct searches for stops and sbottoms are performed in the stop decay channels $\tilde{\mathrm{t}} \to \mathrm{c}\chi$ and $\tilde{\mathrm{t}} \to \mathrm{b}\ell\tilde{\nu}$ and in the sbottom decay channel $\tilde{\mathrm{b}} \to \mathrm{b}\chi$. The results of these searches supersede the ALEPH results reported earlier for data collected at energies up to $\sqrt{s} = 172$ GeV [3]. The D0 experiment [4] has reported a lower limit on the stop mass of 85 GeV/c^2 for the decay into $\mathrm{c}\chi$ and for a mass difference between the $\tilde{\mathrm{t}}$ and the χ larger than about 40 GeV/c^2. Searches for $\tilde{\mathrm{t}} \to \mathrm{c}\chi$, $\tilde{\mathrm{t}} \to \mathrm{b}\ell\tilde{\nu}$ and $\tilde{\mathrm{b}} \to \mathrm{b}\chi$ using data collected at LEP at energies up to $\sqrt{s} = 172$ GeV have also been performed by OPAL [5].

The supersymmetric partners of the light quarks are generally expected in the MSSM to be heavy, i.e., beyond the reach of LEP2, but their masses receive large negative corrections from gluino loops [6]. The dominant decay mode is assumed to be $\tilde{\mathrm{q}} \to \mathrm{q}\chi$. Limits are set on the production of the u, d, s, c, b squarks, under the assumption that they are mass degenerate. The D0 and CDF Collaborations have published limits on degenerate squarks [7, 8]. These limits are outside the LEP2 kinematic range for the case of a light gluino; however limits from LEP2 are competitive with those from the Tevatron if the gluino is heavy.

2 The ALEPH detector

A detailed description of the ALEPH detector can be found in Ref. [9], and an account of its performance as well as a description of the standard analysis algorithms can be found in Ref. [10]. Only a brief overview is given here.

Charged particles are detected in a magnetic spectrometer consisting of a silicon vertex

detector (VDET), a drift chamber (ITC) and a time projection chamber (TPC), all immersed in a 1.5 T axial magnetic field provided by a superconducting solenoid. The VDET consists of two cylindrical layers of silicon microstrip detectors; it performs very precise measurements of the impact parameter in space thus allowing powerful short-lifetime particle tags, as described in Ref. [11]. Between the TPC and the coil, a highly granular electromagnetic calorimeter (ECAL) is used to identify electrons and photons and to measure their energies. Surrounding the ECAL is the return yoke for the magnet, which is instrumented with streamer tubes to form the hadron calorimeter (HCAL). Two layers of external streamer tubes are used together with the HCAL to identify muons. The region near the beam line is covered by two luminosity calorimeters, SICAL and LCAL, which provide coverage down to 34 mrad. The information obtained from the tracking system is combined with that from the calorimeters to form a list of "energy flow particles" [10]. These objects serve to calculate the variables that are used in the analyses described in Section 3.

3 The Analyses

Data collected at $\sqrt{s}$ = 181, 182, 183, and 184 GeV have been analysed, corresponding to integrated luminosities of 0.2, 3.9, 51.0, and 1.9 pb^{-1}, respectively. Three separate analyses are used to search for the processes $\tilde{\mathrm{t}} \to \mathrm{c}\chi$, $\tilde{\mathrm{b}} \to \mathrm{b}\chi$, and $\tilde{\mathrm{t}} \to \mathrm{b}\ell\tilde{\nu}$. All of these channels are characterised by missing momentum and energy. The experimental topology depends largely on Δm, the mass difference between the $\tilde{\mathrm{q}}$ and the χ or $\tilde{\nu}$. When Δm is large, there is a substantial amount of energy available for the visible system and the signal events tend to look like WW, Weν, Zγ^*, and q$\bar{\mathrm{q}}(\gamma)$ events. These processes are characterised by high multiplicity and high visible mass M_{vis}. When Δm is small, the energy available for the visible system is small and the signal events are therefore similar to $\gamma\gamma \to \mathrm{q}\bar{\mathrm{q}}$ events. The process $\gamma\gamma \to \mathrm{q}\bar{\mathrm{q}}$ is characterised by low multiplicity, low M_{vis}, low total transverse momentum p_{t} and the presence of energy near the beam axis. In order to cope with the different signal topologies and background situations, each analysis employs a low Δm selection and a high Δm selection. The values of the analysis cuts are set in an unbiased way following the $\bar{N}_{95}$ procedure [12]. The simulation of the $\gamma\gamma \to \mathrm{q}\bar{\mathrm{q}}$ background is difficult. As a consequence, a safer rejection of this background is ensured by applying tighter cuts than would result from the $\bar{N}_{95}$ procedure.

The analyses used to search for evidence of stop and sbottom production are quite similar to those used at $\sqrt{s}$ = 172 GeV [3] with the addition of b tagging in the channel $\tilde{\mathrm{b}} \to \mathrm{b}\chi$ to further reject the WW, Weν, and Zγ^* background. The differences between the cuts used at $\sqrt{s}$ = 130–172 GeV and the cuts used at $\sqrt{s}$ = 181–184 GeV are described in detail below.

3.1 Search for $\tilde{\mathrm{t}} \to \mathrm{c}\chi$

The process $\mathrm{e^+e^-} \to \tilde{\mathrm{t}}\bar{\tilde{\mathrm{t}}}$ ($\tilde{\mathrm{t}} \to \mathrm{c}\chi$) is characterised by two acoplanar jets and missing mass and energy.

For the small Δm selection, only the thrust and the visible mass cuts needed adjustments. The thrust is required to be less than 0.915 to reduce further the low-multiplicity $\gamma\gamma \to \mathrm{q}\bar{\mathrm{q}}$ background. The lower cut on the visible mass M_{vis}, which is effective against $\gamma\gamma \to \mathrm{q}\bar{\mathrm{q}}$

background, depends upon the mass difference of the signal considered. Since signal events with small Δm tend to have smaller values of $M_{\rm vis}$, the optimal value of this cut decreases as Δm decreases. The visible mass is required to be in excess of 4 GeV/c^2. This cut is raised to 7.5 GeV/c^2 for $\Delta m > 7$ GeV/c^2.

For large Δm, the selection is quite similar to the selection at $\sqrt{s} = 130$–172 GeV. However, a few changes have been made in order to confront the increased level of background from WW, Weν, and Zγ^* that results from the increased luminosity. The $\theta_{\rm scat}$ variable is used to reduce background from Weν. This variable was introduced in Ref. [3] as a means of eliminating $\gamma\gamma \to {\rm q\bar{q}}$ background. Assuming that one of the incoming electrons is scattered while the other one continues undeflected, the polar angle of the scattered electron, $\theta_{\rm scat}$, can then be calculated from the missing transverse momentum $p_{\rm t}$. This variable can also be interpreted in the context of Weν background. The final state of this background typically includes an electron which goes down the beampipe and a neutrino which is within the detector acceptance. In this case, $\theta_{\rm scat}$ is an estimate of the neutrino polar angle which tends to be large for the Weν background. For the signal process, $\theta_{\rm scat}$ tends to be smaller, as long as Δm is not too large. The optimal value of this cut for a hypothesis of $\Delta m < 35$ GeV/c^2 is $\theta_{\rm scat} < 60^\circ$, while for a hypothesis of $\Delta m > 35$ GeV/c^2 the cut is not applied.

Background from WW, Weν, and Zγ^* is also addressed by tightening the $M_{\rm vis}/\sqrt{s}$ cut. This cut also depends on the Δm of the signal being considered. A hypothesis on Δm=15 GeV/c^2 gives an optimal cut of $M_{\rm vis}/\sqrt{s} < 0.25$, while a hypothesis on Δm=35 GeV/c^2 gives an optimal cut of $M_{\rm vis}/\sqrt{s} < 0.33$. Finally, the optimal cut for all Δm greater than 50 GeV/c^2 is $M_{\rm vis}/\sqrt{s}$ < 0.35.

Selection efficiency and background

According to the $\bar{N}_{95}$ procedure, the low Δm selection is used for $\Delta m < 15$ GeV/c^2, while for $\Delta m \geq 15$ GeV/c^2, the high Δm selection is used. The changeover occurs at a larger Δm value than for $\sqrt{s} = 130$–172 GeV, where it was $\Delta m = 10$ GeV/c^2, due to the larger contamination in the high Δm selection.

The $\tilde{\rm t} \to {\rm c}\chi$ efficiencies are shown in Figure 1a; the discontinuity at $\Delta m = 15$ GeV/c^2 is due to the switching between the low and high Δm selections.

The background to the low Δm selection is dominated by $\gamma\gamma \to {\rm q\bar{q}}$ and $\gamma\gamma \to \tau^+\tau^-$ and has a total expectation of 1.5 events (~ 30 fb) for the looser value of the lower $M_{\rm vis}$ cut. For the high Δm selection, the background is dominated by WW, Weν, Zγ^*, and ${\rm q\bar{q}}(\gamma)$. If the upper cut on $\theta_{\rm scat}$ is not applied and the loosest value of the upper cut on $M_{\rm vis}$ is applied, the total background expectation for the high Δm selection is 3.5 events (~ 60 fb).

3.2 Search for $\tilde{\rm b} \to {\rm b}\chi$

The experimental topology of the ${\rm e^+e^-} \to \tilde{\rm b}\bar{\tilde{\rm b}}$ ($\tilde{\rm b} \to {\rm b}\chi$) process is characterised by two acoplanar b jets and missing mass and energy. Both the low and high Δm selections use the same selection criteria against $\gamma\gamma \to {\rm q\bar{q}}$ background as at lower energies [3] with cuts rescaled to the centre-of-mass energy when appropriate. Only the cuts against WW, Zγ^*, and

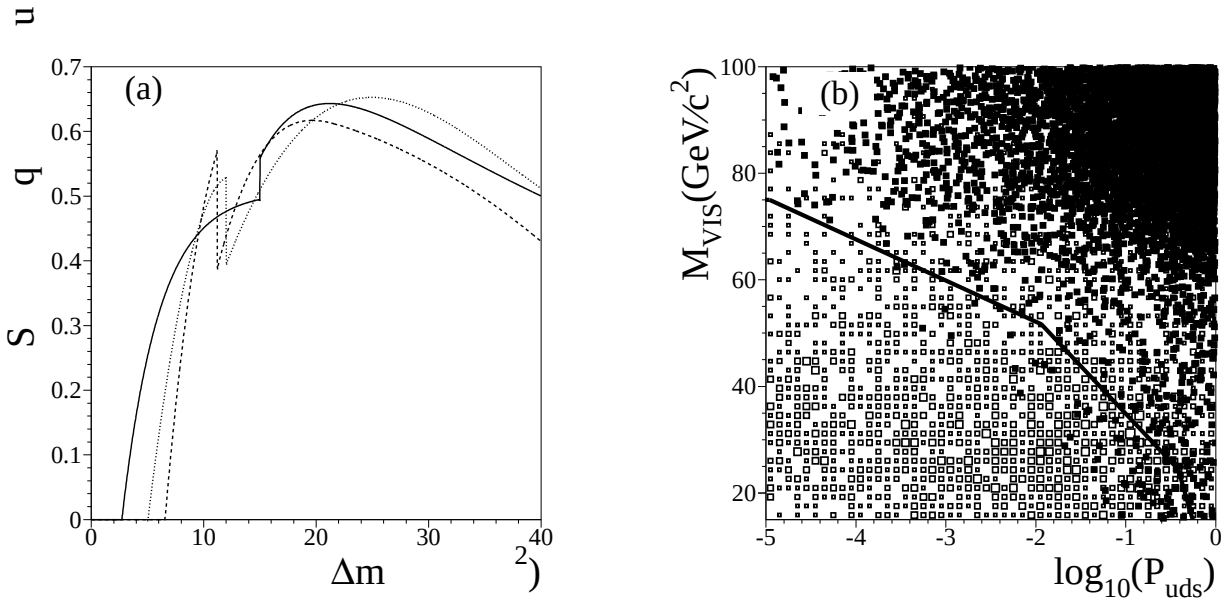

Figure 1: (a) Efficiencies as a function of Δm: for an 80 GeV/c^2 stop decaying as $\tilde{t} \to c\chi$ (solid curve), for an 80 GeV/c^2 stop decaying as $\tilde{t} \to b\ell\tilde{\nu}$ (dashed curve), and an 80 GeV/c^2 sbottom decaying as $\tilde{b} \to b\chi$ (dotted curve). (b) Two-dimensional cut in the plane $M_{\rm vis}$-$\log_{10}(P_{\rm uds})$. Signal (open squares) and background (solid squares) distributions are also shown.

Weν have been reoptimized. Most of the cuts are similar to those used for the $\tilde{t} \to c\chi$ process; here only the differences will be described.

For the low Δm selection, the visible mass of the event is required to be greater than 7.5 GeV/c^2. In this channel the b quark in the final state produces a visible mass higher than in the $\tilde{t} \to c\chi$ channel.

For the high Δm selection, the level of WW, Zγ^* and Weν background was reduced by taking advantage of the lifetime content of the $\tilde{b} \to b\chi$ topology. The b quark events were tagged by using the b-tag event probability ($P_{\rm uds}$) described in [11]. Since this probability depends largely on the b jet boost, events are more b-like as the event visible mass increases. A two-dimensional cut is applied in the $M_{\rm vis}$ vs $\log_{10}(P_{\rm uds})$ plane (Figure 1b); starting from a loose value of the b-tag cut when the visible mass is low, the cut becomes tighter for larger values of visible mass.

Selection efficiency and background

According to the $\bar{N}_{95}$ procedure, for $\Delta m < 12$ GeV/c^2 the low Δm selection is used while for $\Delta m > 12$ GeV/c^2 the high Δm selection is used. The efficiency is shown in Figure 1a, as a function of Δm for $M_{\tilde{b}}$=80 GeV/c^2. The total background expectation for the low Δm selection is 1.1 events (20 fb), and dominated by $\gamma\gamma \to q\bar{q}$. For the high Δm selection the WW, Zγ^*, and Weν background is highly suppressed by b tagging and the total background expectation

is 0.6 events (10 fb).

3.3 Search for $\tilde{t} \to b\ell\tilde{\nu}$

The experimental signature for $e^+e^- \to \tilde{t}\bar{\tilde{t}}$ ($\tilde{t} \to b\ell\tilde{\nu}$) is two acoplanar jets plus two leptons with missing momentum.

For the low Δm selection, the p_t cut used at 172 GeV is reinforced by requiring that the p_t calculated without neutral hadrons and the p_t calculated with only charged tracks both be greater than $0.75\%\sqrt{s}$.

For the large Δm selection, the cuts are optimised in order to confront the increased rate of WW and $Z\gamma^*$ backgrounds at 183 GeV. Only two cut values are changed with respect to their values at 172 GeV. First, the upper cut on the hadronic mass is tightened: the hadronic mass is required to be less than $25\%\sqrt{s}$ if one lepton is identified and less than $20\%\sqrt{s}$ if more than one lepton is identified. Additionally, the cut on the leading lepton isolation is reinforced: the energy in a 30° cone around the direction of the electron or muon momentum must be smaller than 2.7 times the electron or muon energy.

Selection efficiency and background

The combination of the two selections is chosen according to the $\bar{N}_{95}$ procedure. For $\Delta m < 11$ GeV/c^2, the logical OR of the two selections is used: the high Δm selection helps to recover efficiency while leaving the background level unchanged. For $\Delta m \geq 11$ GeV/c^2, only the high Δm selection is used. This is in contrast to the situation for the 130–172 GeV data; because the background was low for both the low and the high Δm selections, the OR of the two selections was optimal for all Δm.

The $\tilde{t} \to b\ell\tilde{\nu}$ selection efficiencies are given in Figure 1a. The effect of switching from the OR of the two selections to the high Δm selection by itself can be seen at $\Delta m = 11$ GeV/c^2. The background to the low Δm selection is dominated by $\gamma\gamma \to q\bar{q}$ and has a total expectation of 0.8 events (~ 14 fb). For the high Δm selection, the very low expected background (0.1 events expected or $\sim$2 fb) is dominated by WW events.

3.4 Systematic uncertainties

The systematic uncertainties on the $\tilde{t}$ and $\tilde{b}$ selection efficiencies originating from the physical processes in the Monte Carlo simulation as well as those related to detector effects are evaluated following the procedure described in Reference [3]. The relative uncertainty on the selection efficiency in the case of $\tilde{t} \to c\chi$ is 13% for low Δm and 6% for high Δm; in the case of $\tilde{t} \to b\ell\tilde{\nu}$ it is 16% for low Δm and 6% for high Δm; for the $\tilde{b} \to b\chi$ channel it is 12% for low Δm and 6% for high Δm. These errors are dominated by the uncertainties on the simulation of $\tilde{t}$ and $\tilde{b}$ production and decay. An additional source of systematic error for the high Δm $\tilde{b} \to b\chi$ selection efficiency derives from the uncertainty on the b-tagging. This systematic uncertainty has been studied by measuring R_b as a function of the b-tag cut in the calibration data collected at the Z peak during the 1997 run. The total uncertainty on the efficiency for the high Δm

$\tilde{b} \to b\chi$ selection is 7%. The systematic uncertainties are included in the final result following the method described in [13].

4 Results

A total of five events are selected by the $\tilde{t} \to c\chi$ analysis, four by the high Δm selection and one by the low Δm selection. This is consistent with the 3.5 events expected in the high Δm selection and the 1.5 events expected in the low Δm selection. The kinematic properties of the high Δm events are all consistent with $Z\gamma^*$, WW, or $We\nu$, while the kinematic properties of the low Δm event suggest the process $\gamma\gamma \to q\bar{q}$.

A single event is selected by the $\tilde{b} \to b\chi$ analysis. This event, which is found by the high Δm selection, is also found by the $\tilde{t} \to c\chi$ high Δm selection. The three high Δm $\tilde{t}$ candidates not selected by the sbottom analysis are all rejected by the b-tag. The number of events selected in the data is consistent with the expectation from background processes (1.1 from the low and 0.6 from the high Δm selections).

A single event is also selected by the $\tilde{t} \to b\ell\tilde{\nu}$ analysis. The event is found by the low Δm selection, and is consistent with $\gamma\gamma \to q\bar{q}$ production. The total of one event selected is consistent with the 0.9 events that are expected from background processes (0.8 from the low and 0.1 from the high Δm selections).

Since no evidence for the production of $\tilde{t}$ or $\tilde{b}$ is found, it is appropriate to set lower limits on their masses. The limits are extracted without background subtraction. Figures 2a and 2b give the 95% C.L. excluded regions for the channel $\tilde{t} \to c\chi$. For this channel, the $\theta_{\tilde{t}}$-independent lower limit on $m_{\tilde{t}}$ is 74 GeV/c^2, assuming a mass difference between the $\tilde{t}$ and the χ of 10–40 GeV/c^2, corresponding to a large part of the region not excluded by the D0 search. Figures 3a and 3b give the excluded regions for the $\tilde{t} \to b\ell\tilde{\nu}$ channel, assuming equal branching ratios for the $\tilde{t}$ decay to e, μ and τ. In this case, the $\theta_{\tilde{t}}$-independent lower limit on $m_{\tilde{t}}$ is 82 GeV/c^2, assuming a mass difference between the $\tilde{t}$ and the $\tilde{\nu}$ of at least 10 GeV/c^2, and using also the LEP1 exclusion on the sneutrino mass.

Figures 4a and 4b give the excluded regions for the $\tilde{b}$ in the decay channel $\tilde{b} \to b\chi$. A lower limit of 79 GeV/c^2 is set on $m_{\tilde{b}}$, assuming that $\theta_{\tilde{b}}$ is 0° and that the mass difference between the $\tilde{b}$ and the χ is at least 10 GeV/c^2. Figure 4b shows that only a restricted region is excluded when $\theta_{\tilde{b}}$ =68°. When decoupling from the Z occurs, sbottoms can only be produced through photon exchange and the cross section for the $\tilde{b}$ (charge $-1/3$) is four times lower than the cross section for the $\tilde{t}$ (charge $+2/3$).

Limits on degenerate squarks

Here the decay $\tilde{q} \to q\chi$ is assumed to be dominant. It has a topology similar to that of $\tilde{t} \to c\chi$. The $\tilde{t} \to c\chi$ analysis can therefore be used to search for generic squark production. In order to check the efficiency of the $\tilde{t} \to c\chi$ selection when it is applied to degenerate squark production, samples of the process $\tilde{q} \to q\chi$ were generated and run through the full ALEPH detector simulation. As expected, the selection efficiency for these samples is similar to the

selection efficiency for the corresponding $\tilde{t} \to c\chi$ samples. The $\tilde{q} \to q\chi$ efficiencies were then parametrised as a function of squark mass and Δm, and this parametrization is used to set the limits on generic squark production. For q = u, d, s, or c, the mixing between $\tilde{q}_R$ and $\tilde{q}_L$ is expected to be negligible. The mixing between $\tilde{b}_R$ and $\tilde{b}_L$ is also assumed to be negligible in the case that the sbottoms are mass degenerate with the partners of the four lightest quarks.

Figure 5a shows the exclusion curves assuming five degenerate squark flavours. In the more conservative curve, only $\tilde{q}_R\bar{\tilde{q}}_R$ production is allowed, while in the other curve, both $\tilde{q}_R\bar{\tilde{q}}_R$ and $\tilde{q}_L\bar{\tilde{q}}_L$ production are allowed, assuming that $\tilde{q}_L$ and $\tilde{q}_R$ are mass degenerate. For these curves the efficiency parametrisation developed for the dedicated sbottom search has been applied to the processes $e^+e^- \to \tilde{b}_R\bar{\tilde{b}}_R$ and $e^+e^- \to \tilde{b}_L\bar{\tilde{b}}_L$.

Searches for degenerate squarks have been performed by CDF and D0 at the Tevatron; the resulting limits in the gluino-squark mass plane are shown in Figure 5b. While these experiments can exclude quite an extensive region of this plane, there is an uncovered region in the exclusion for large gluino masses.

In the MSSM, when GUT relation are assumed, the neutralino mass can be related to the gluino mass once the values of μ and $\tan\beta$ are fixed. Therefore, ALEPH limits in the squark-neutralino mass plane can be translated to the gluino-squark mass plane. The ALEPH results are shown in Figure 5b assuming the values of μ and $\tan\beta$ used by CDF ($\tan\beta = 4$ and $\mu = -400$ GeV/c^2). This exclusion is affected only slightly if the D0 set of values ($\tan\beta = 2$ and $\mu = -250$ GeV/c^2) is used instead.

The limit on $m_{\tilde{q}}$ is at least 87 GeV/c^2 up to $m_{\tilde{g}} \sim 545$ GeV/c^2 (535 GeV/c^2 if D0 values are used). At this point, $m_\chi = 82$ GeV/c^2 and the mass difference between $\tilde{q}$ and χ is only 5 GeV/c^2. Beyond these points, the $\tilde{t} \to c\chi$ analysis is no longer sensitive to the production of degenerate squarks.

5 Conclusions

Searches have been performed for scalar quarks at $\sqrt{s} = 183$ GeV. Five candidate events are observed in the $\tilde{t} \to c\chi$ channel, one in the $\tilde{t} \to b\ell\tilde{\nu}$ channel, and one in the $\tilde{b} \to b\chi$ channel. These totals are consistent with the expectation from background processes.

A 95% C.L. limit of $m_{\tilde{t}} > 74$ GeV/c^2 is obtained from the $\tilde{t} \to c\chi$ search, independent of the mixing angle and for $10 < \Delta m < 40$ GeV/c^2. From the $\tilde{t} \to b\ell\tilde{\nu}$ channel, the $\theta_{\tilde{t}}$-independent limit $m_{\tilde{t}} > 82$ GeV/c^2 is established, if the mass difference between the $\tilde{t}$ and the $\tilde{\nu}$ is greater than 10 GeV/c^2 and for equal branching ratios of the $\tilde{t}$ into e, μ, and τ.

A limit is also obtained for the $\tilde{b}$ decaying as $\tilde{b} \to b\chi$. The limit is $m_{\tilde{b}} > 79$ GeV/c^2 for the supersymmetric partner of the left-handed state of the bottom quark if the mass difference between the $\tilde{b}$ and the χ is greater than 10 GeV/c^2.

Finally, limits are also derived for the supersymmetric partners of the light quarks. Assuming five degenerate flavours and the production of both "left-handed" and "right-handed" squarks, a limit of $m_{\tilde{q}} > 87$ GeV/c^2 is set. This limit is valid for $\Delta m > 5$ GeV/c^2. Using the GUT relations, for $\tan\beta = 4$ and $\mu = -400$ GeV/c^2, the limit of $m_{\tilde{q}} > 87$ GeV/c^2 is valid for gluino masses smaller than 545 GeV/c^2.

6 Acknowledgements

We wish to congratulate our colleagues from the accelerator divisions for the continued successful operation of LEP at high energies. We would also like to express our gratitude to the engineers and support people at our home institutes without whom this work would not have been possible. Those of us from non-member states wish to thank CERN for its hospitality and support.

References

[1] For a review see: Ed. M. Jacob, *Supersymmetry and Supergravity.* North-Holland and World Scientific, 1986.

[2] K. Hikasa and M. Kobayashi, Phys. Rev. **D 36** (1987) 724;
M. Drees and K. Hikasa, Phys. Lett. **B 252** (1990) 127.

[3] ALEPH Collaboration, *Search for Scalar Top and Scalar Bottom Quarks at LEP2.* Phys. Lett. **B 413** (1997) 431.

[4] D0 Collaboration, *Search for Light Top Squarks in $p\bar{p}$ Collisions at $\sqrt{s} = 1.8$ TeV.* Phys. Rev. Lett. **76** (1996) 2222.

[5] OPAL Collaboration, *Search for Scalar Top and Scalar Bottom Quarks at $\sqrt{s}$= 170 GeV - 172 GeV in e^+ e^- Collisions.* Z. Phys. **C 75** (1997) 409.

[6] A. Donini, Nucl. Phys. **B 467** (1996) 3.

[7] D0 Collaboration, *Search for Squarks and Gluinos in $p\bar{p}$ Collisions at $\sqrt{s} = 1.8$ TeV.* Phys. Rev. Lett. **75** (1995) 618.

[8] CDF Collaboration, *Search for gluinos and squarks at the Fermilab Tevatron collider.* Phys. Rev. **D 56** (1997) 1357.

[9] ALEPH Collaboration, *ALEPH: A detector for electron-positron annihilation at LEP.* Nucl. Instrum. and Methods **A 294** (1990) 121.

[10] ALEPH Collaboration, *Performance of the ALEPH detector at LEP.* Nucl. Instrum. and Methods **A 360** (1995) 481.

[11] ALEPH Collaboration, *A Precise Measurement of $\Gamma_{Z\to b\bar{b}}/\Gamma_{Z\to hadrons}$.* Phys. Lett. **B 313** (1993) 535.

[12] ALEPH Collaboration, Phys. Lett. **B 384** (1996) 427;
G. F. Grivaz and F. Le Diberder, LAL **92-37** (1992).

[13] R.D. Cousins and V.L. Highland, Nucl. Instrum. and Methods **A 320** (1992) 331.

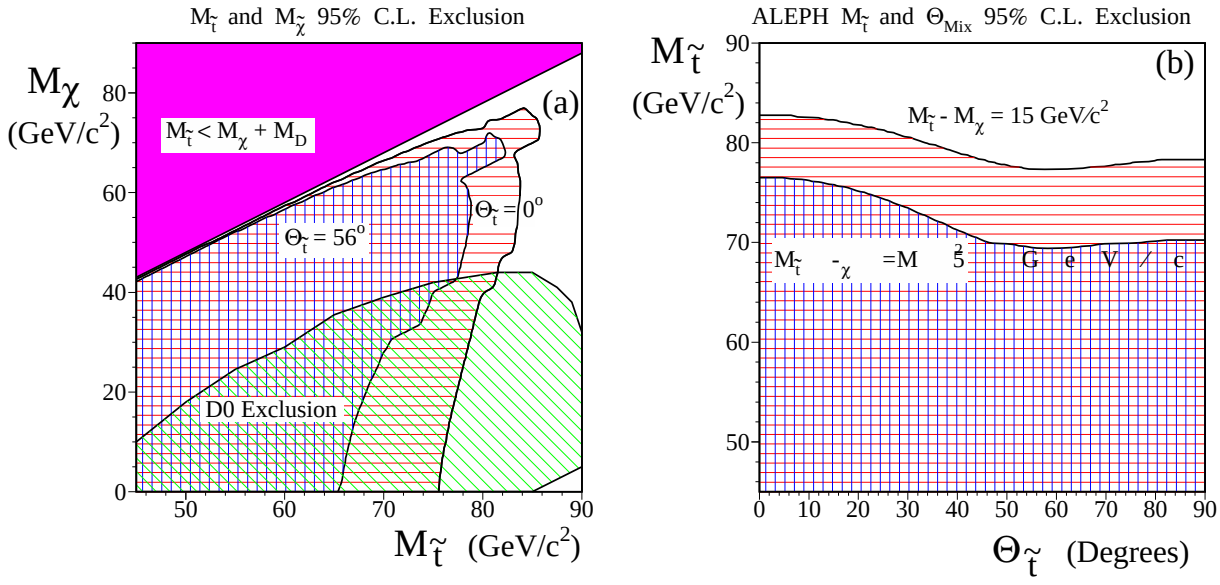

Figure 2: Excluded regions for $\tilde{t} \to c\chi$. (a) Excluded region in the m_χ vs $m_{\tilde{t}}$ plane; the region excluded by the D0 collaboration is also indicated. (b) Excluded region in the $m_{\tilde{t}}$ vs $\theta_{\tilde{t}}$ plane. In (a), the excluded regions are given for $\theta_{\tilde{t}}$=0°, corresponding to maximum $\tilde{t}$-Z coupling, and for $\theta_{\tilde{t}}$=56°, corresponding to minimum $\tilde{t}$-Z coupling.

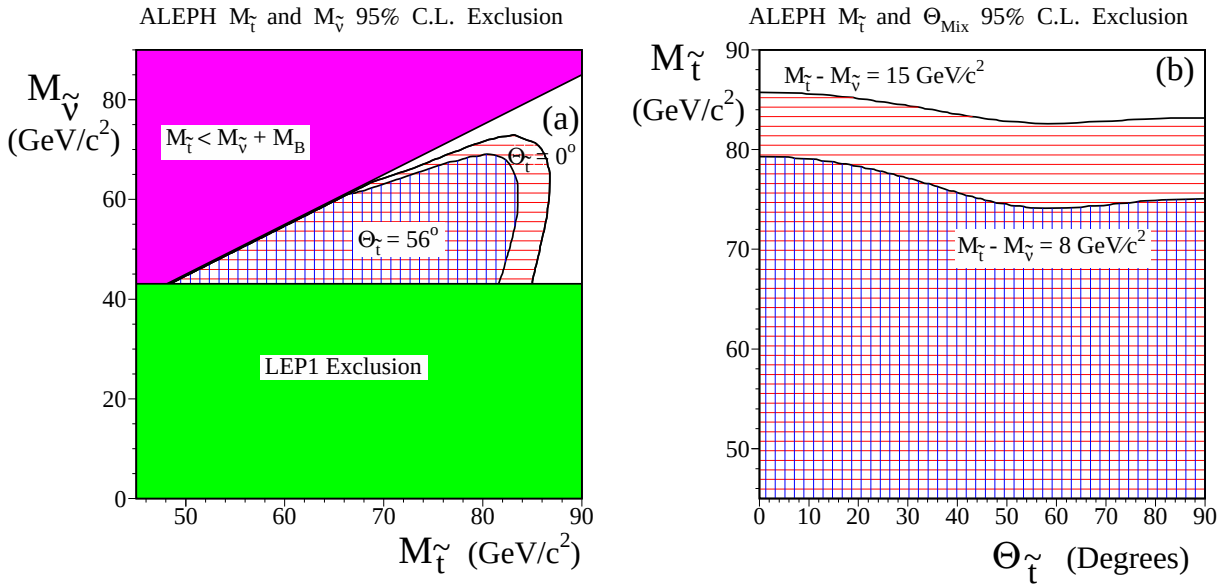

Figure 3: Excluded regions for $\tilde{t} \to b\ell\tilde{\nu}$ (equal branching fractions for the $\tilde{t}$ decay to e, μ, and τ are assumed). (a) Excluded region in the $m_{\tilde{\nu}}$ vs $m_{\tilde{t}}$ plane. (b) Excluded region in the $m_{\tilde{t}}$ vs $\theta_{\tilde{t}}$ plane. In (a), the excluded regions are given for $\theta_{\tilde{t}}$=0°, corresponding to maximum $\tilde{t}$-Z coupling, and for $\theta_{\tilde{t}}$=56°, corresponding to minimum $\tilde{t}$-Z coupling. Also shown in (a) is the region excluded from LEP1 data, i.e., the $\tilde{\nu}$ mass limit obtained from the measurement of the Z lineshape.

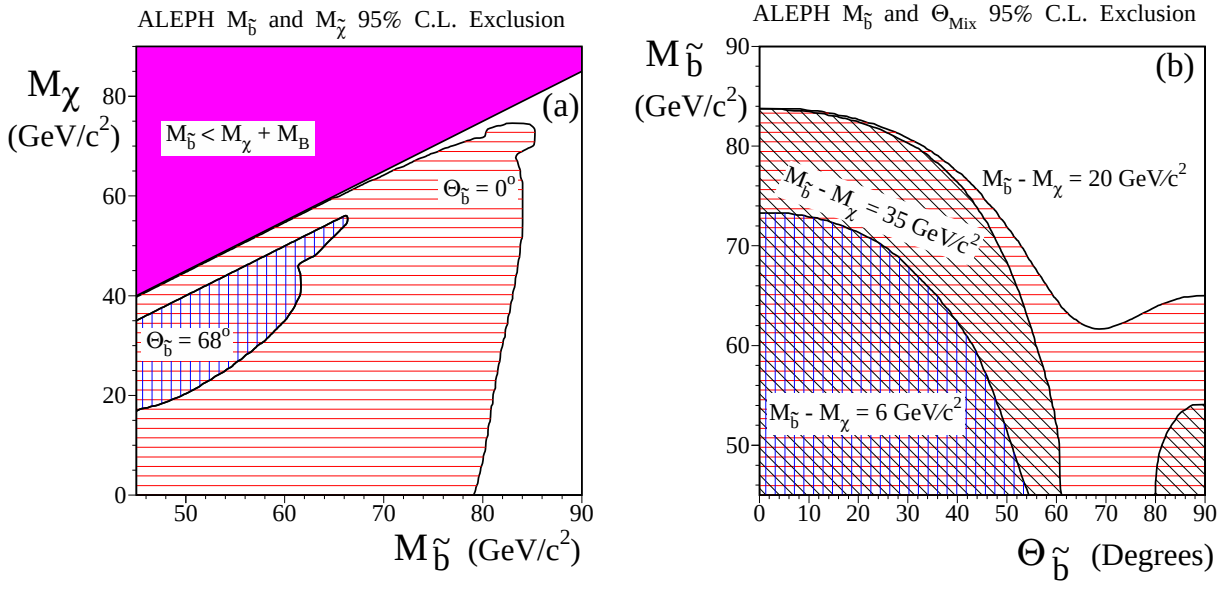

Figure 4: Excluded regions for $\tilde{b} \to b\chi$. (a) Excluded region in the m_χ vs $m_{\tilde{b}}$ plane. (b) Excluded region in the $m_{\tilde{b}}$ vs $\theta_{\tilde{b}}$ plane. In (a), the excluded regions are given for $\theta_{\tilde{b}}$=0°, corresponding to maximum $\tilde{b}$-Z coupling, and for $\theta_{\tilde{b}}$=68°, corresponding to minimum $\tilde{b}$-Z coupling.

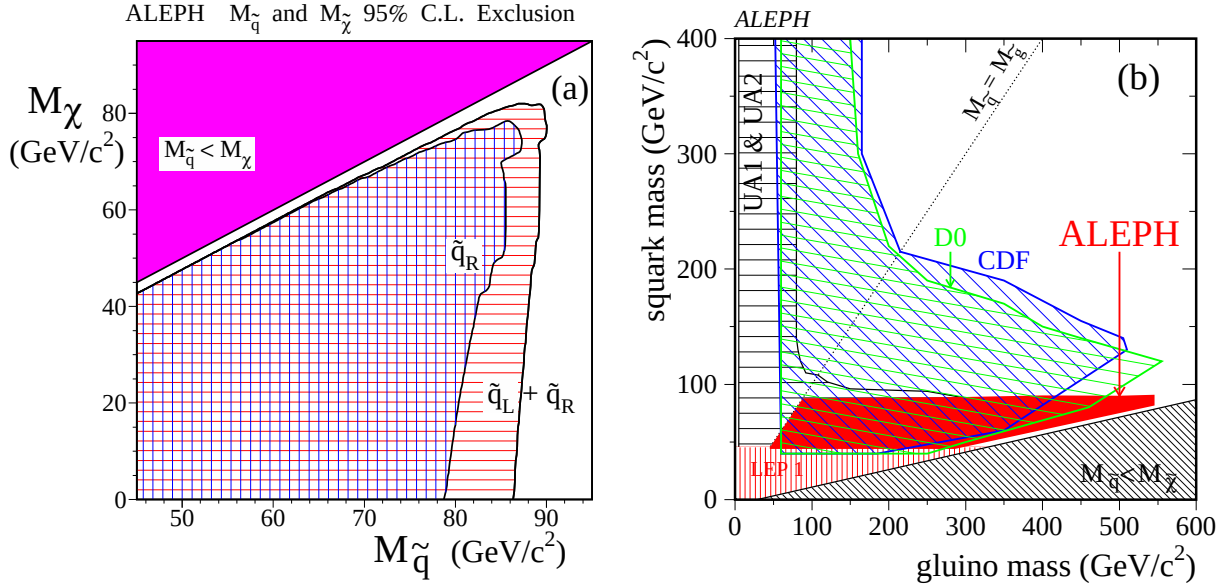

Figure 5: (a) Excluded region for the supersymmetric partners of the u, d, s, c, and b quarks, assuming the squarks to be degenerate in mass. In (a), two curves are given: one curve assumes that only $\tilde{q}_R$ is accessible at LEP2 energies, while the other curve assumes that $\tilde{q}_R$ and $\tilde{q}_L$ are both accessible at LEP2 energies. (b) The ALEPH result for five degenerate flavours, $\tilde{q}_R$ and $\tilde{q}_L$ production, shown in the gluino-squark mass plane for $\tan\beta = 4$ and $\mu = -400\,\mathrm{GeV}/c^2$. This result excludes a small region not excluded by CDF and D0.